DOI: 10.1002/ejic.200900078

High-Density Magnetite Nanoparticles Located in Carbon Hollow Microspheres with Good Dispersibility and Durability: Their One-Pot Preparation and Magnetic Properties

Rongbo Zheng,[a,b] Xianwei Meng,[a] and Fangqiong Tang*[a]

Keywords: Materials science / Nanostructures / Magnetic properties / Hollow spheres / Iron / Magnetite

We report, for the first time, a one-step, rapid, template-free and continuous strategy for synthesising high-density magnetite (Fe_3O_4) nanoparticles located in carbon hollow microspheres (MCHMs) in which Fe_3O_4 nanoparticles (8–20 nm) are randomly dispersed in the shells of carbon hollow microspheres. The synthesis is achieved through ultrasonic spray pyrolysis of aqueous solutions containing ferrous chloride and citric acid. Interestingly, it was found that there are some pores (2–6 nm) in the carbon shell. Magnetic hysteresis loop measurements show that the saturation magnetisation of MCHMs is as high as 48.2 emu g^{-1} which probably makes them more pliable to manipulation by the external magnetic field. Most importantly, because of the presence of carbon on their surfaces, MCHMs not only exhibit good resistance to acid but can also be easily dispersed in both polar and non-polar solvents.

Introduction

Recently, magnetic (especially Fe_3O_4) hollow spheres with tailored structures and surface properties have attracted great attention because of their interesting characteristics such as their reduced density which thwarts the density limitations met in various applications. Other characteristics include being able to combine the controlled release and diagnosis in one system by means of filling the inner void with target drugs as well as other wide applications in catalysis and biotechnology, etc.[1–6] Nevertheless, it should also be borne in mind that for high performance in function-specific biological or separation applications, magnetic hollow spheres should be biocompatible, have a high magnetic saturation to provide maximum signal, good dispersion in various solvents and be stable under acidic or basic conditions. To meet the aforementioned requirements, much effort has been devoted to developing various protection strategies, including functionalising of organic species (surfactants or polymers)[7–10] or coating with an inorganic shell (e.g. silica).[11–13] Compared with the polymer or silica component, carbon[14–18] materials have attracted wider attention because they have particular advantages such as higher stability and better conductivity over polymers or silica.[19–21] Although polymer- or silica-magnetite hollow spheres have been successfully prepared by several methods,[2,7,10,11] the literature on the synthesis of carbon-magnetite hollow spheres is scarce.[14,22] For instance, carbonaceous-wüstite composite hollow microspheres have been synthesised by means of a novel shape fabrication process based on simple ion-exchange reactions between microspheres of ion-exchange resins and $K_3[Fe(C_2O_4)_3]$ followed by thermal treatment of the resultant resin derivative under an inert atmosphere.[14]

Fuertes et al. have designed a multiple-step route for synthesising hollow magnetic mesoporous spheres made up of ferrite (e.g. Fe_3O_4) nanoparticles incorporated in a mesoporous carbon shell.[22] However, the intrinsically complicated precursors and the requirement of a template and long curing times in the above method are not suitable for continuous production on a large scale. Also, the saturation magnetisation (M_s) of the above carbon-magnetite hollow composites is relative low (< 20 emu g^{-1}). Therefore, the development of a convenient and template-free approach to the synthesis of high-density Fe_3O_4 nanoparticles located in carbon hollow microspheres (MCHMs) with high stability, dispersibility, and M_s is desirable.

As a simple and continuous technology, ultrasonic spray pyrolysis (USP) has long been used in industry or the laboratory for the production of spherical powders including metal oxides, sulfides and carbon etc.[23–28] In this study, we exploited the USP route to synthesise MCHMs using aqueous solutions containing ferrous chloride and citric acid as precursors. The formation mechanism is based on the phenomenon that the surface enrichment of some components (i.e., formation of hollow spheres) would take place

[a] Technical Institute of Physics and Chemistry,
Chinese Academy of Sciences,
Beijing 100190, P. R. China
Fax: +86-10-62554670
E-mail: Tangfq@mail.ipc.ac.cn
[b] Graduate School of the Chinese Academy of Sciences,
Beijing 100039, P. R. China
Supporting information for this article is available on the WWW under http://dx.doi.org/10.1002/ejic.200900078.

when multicomponent aerosol droplets were pyrolysed.[11,23] Thus, the approach presented here is one-step, rapid, continuous and template-free. Due to the presence of carbon, the prepared MCHMs exhibit good acid resistance and dispersibility which indicates potential applications in the immobilisation of enzymes,[22] separation of pollutants from water,[29] extraction of DNA[30] and in catalyst supports, etc.

Results and Discussion

In the present route, ultrasound is used to produce aerosol droplets dispersed in nitrogen by means of ultrasonic spray treatment of the precursor aqueous solutions. As the aforementioned aerosol droplets are carried in a nitrogen stream through a quartz-glass tube in a hot furnace, water evaporation and precursor decomposition occurs generating MCHMs. With USP, the aerosol droplets act as individual micrometer-sized chemical reactors to impose morphology control on the target products.[23–28]

Herein, aqueous solutions of ferrous chloride and citric acid were used as precursors to form MCHMs by using USP. The morphology of the product was investigated by scanning electron microscopy (SEM) and transmission electron microscopy (TEM). The overall morphology of sample HC 2 is revealed in Figure S1 which indicates that the sample is composed of a large quantity of microspheres with sizes in the range of 1–3 μm. From Figure 1 (A) we can see that the obtained microspheres exhibit a hollow structure with obvious contrast between the dark edge and the pale centre. The magnified image (Figure 1, B–D) indicates that high-density Fe_3O_4 nanoparticles (8–20 nm) are randomly dispersed in the shells of the hollow spheres. In general, there are three kinds of morphologies: double-layer bowls, hollow spheres and bubble-like spheres. In some cases, the hollow spheres are caved due to their thin walls. Moreover, there are some double-layer bowls which are formed through the collision of thinner hollow spheres (the thickness of wall is about 20 nm) with the others (the thickness of wall is about 40 nm) as shown in parts A and C of Figure 1. When the thickness of the wall (e.g. 40 nm) is sufficient, the hollow spheres would remain intact during their collision (Figure 1, B). Bubble-like spheres are comprised of several small hollow spheres encapsulated in one big sphere. The distribution of Fe_3O_4 nanoparticles in the carbon matrix can be further investigated by removing Fe_3O_4 nanoparticles under acidic conditions. As shown in Figure 2, porous hollow carbon spheres with pores (about 10 nm) were formed when sample HC 2 was treated with concentrated HCl solution (12 M) for 12 h. We speculate that one Fe_3O_4 nanoparticle generates one pore during the acidic treatment. Thus, we can confirm that Fe_3O_4 nanoparticles (about 10 nm) are randomly dispersed in the shells of MCHMs (Figure 1).

Figure 3 shows the X-ray diffraction (XRD) pattern of the aforementioned MCHMs (sample HC2). As shown in Figure 3, all the diffraction peaks can be indexed to face-centred cubic Fe_3O_4 (JCPDS file No. 48–1487) or cubic γ-Fe_2O_3 (JCPDS file No. 39–1346). No obvious impurity phase, such as nonmagnetic α-Fe_2O_3, can be detected in Figure 3 (A). Figure S2 shows the XRD pattern of the product after treatment with concentrated HCl (12 M) and this can be indexed as pure hexagonal graphite.[17] The mean crystallite size of Fe_3O_4 is about 15 nm and this was evaluated from full-width half-maximum (FWHM) of the (311) plane using the Scherrer equation. As shown in Figure S3, we focussed electrons on one sphere to perform the SEM-energy-dispersive X-ray analysis (EDX). The result of EDX (Figure 3, B) indicates that the atomic ratio of Fe/O (31.82/43.04) is consistent with that of the theoretical calculation result of Fe_3O_4 which demonstrates that iron oxide should be indexed to face-centred cubic Fe_3O_4 instead of γ-Fe_2O_3. The element Si can be ascribed to the silicon wafer that supports the sample. Thermogravimetric analysis (TGA) was performed to obtain the composition of sample HC 2. There is a phenomenon of an increase in mass between 182 and 280 °C (Figure S3). It was deduced that Fe_3O_4 is oxidised to form Fe_2O_3 in air which further reveals that iron oxide should be Fe_3O_4 instead of γ-Fe_2O_3. From Figure S4, we can calculate that the Fe_3O_4 and carbon contents in sample HC 2 are about 70.9 and 29.1 wt.-%, respectively.

The porous characteristics of sample HC2 were characterised by nitrogen physisorption. The N_2 adsorption-desorption isotherm exhibits a hysteresis loop in the relative

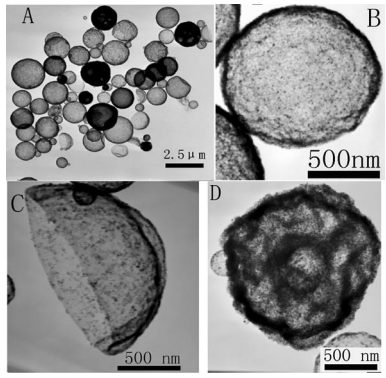

Figure 1. Images of MCHMs (HC 2): (A) TEM images showing the overall morphology; high-magnification TEM images of (B) intact hollow sphere; (C) double-layer bowl; (D) bubble-like sphere.

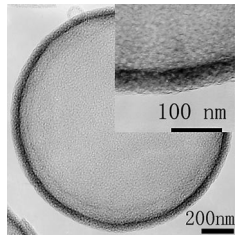

Figure 2. TEM images of porous hollow carbon spheres obtained by acid treatment of sample HC 2 in concentrated HCl (12 M) for 12 h.

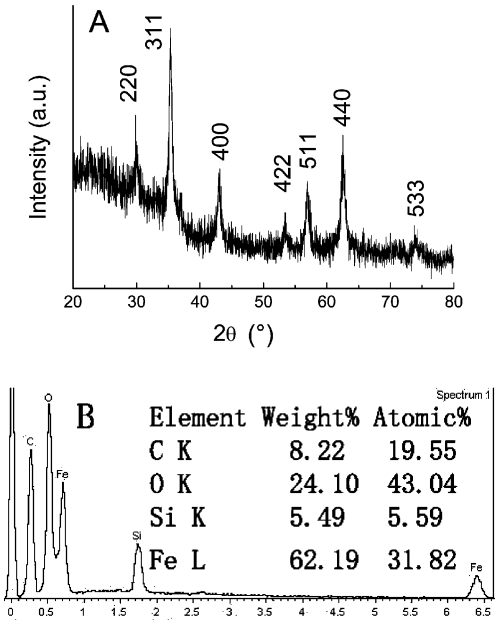

Figure 3. XRD patterns (A) and EDS (B) of MCHMs (HC 2) prepared by USP.

pressure (P/P^0) range of 0.45–0.9 (Figure 4, A) with a Brunauer-Emmett-Teller (BET) surface area of 36.4 $m^2 g^{-1}$. As illustrated by the pore size distribution displayed in Figure 4 (B), this porosity consists of mesopores with sizes of 2–6 nm (two distinct pore distribution peaks at 2.6 and 4.0 nm). The Barett-Joyner-Halenda (BJH) desorption average pore size is 7.0 nm and the single-point adsorption total volume at P/P_0 = 0.994 is 0.083 $cm^3 g^{-1}$.

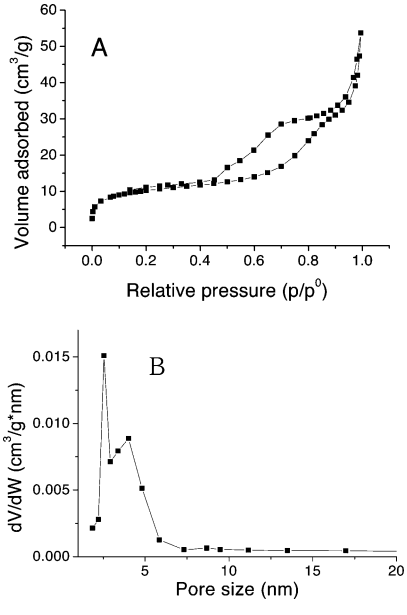

Figure 4. (A) Nitrogen adsorption isotherm and (B) pore size distributions of sample HC 2.

In order to investigate the formation mechanism of MCHMs, controlled experiments were carried out. No black product could be obtained if an aqueous solution of citric acid was used as a precursor. A brick-red product was generated by USP of aqueous ferrous chloride (HC 0). The results of SEM revealed that crushed hollow spheres were formed (data not show). When a saturated aqueous ferric citrate solution was used as a precursor (HC 3), carbon-magnetite hollow microspheres (similar to sample HC 2) were formed. As shown in Table 1, the initial concentration of ferrous chloride had little effect on the C/Fe atomic ratio in the MCHMs (HC 1 and 2) which meant both carbon and Fe_3O_4 may be in situ generated from the pyrolysis of iron citrate (formed in the reaction between citric acid and ferrous chloride) (Figure 5).

Table 1. Synthetic conditions for preparation of the samples.

Sample	Reactant and concentration		Morphology[b]	The average atom ratio C:Fe[c]
	$FeCl_2$	citric acid		
HC 0	0.08 M		C-hollow	
HC 1	0.08 M	0.4 M	hollow	34.1:65.9
HC 2	0.56 M	0.4 M	hollow	38.1:61.9
HC 3[a]			hollow	

[a] Only saturated aqueous ferric citrate was used as a precursor. [b] C-Hollow indicates crushed-hollow spheres. [c] The average atom ratio of C/Fe was measured by EDS.

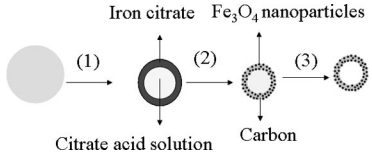

Figure 5. Proposed formation mechanism of MCHMs by USP.

Based on the above discussions, the following scenario can be envisioned for the formation of MCHMs (Figure 4). (1) The rapid evaporation of water favours the surface precipitation of dissolved components. The low solubility of iron citrate compared with that of free citric acid, promotes the initial precipitation of the iron citrate solid shell. (2) When the droplet temperature increases, the exterior iron citrate decomposes to generate magnetite and carbon. However, the interior citric acid does not decompose as revealed by the fact that no carbon formed by USP originated from a single citric acid aqueous solution. (3) MCHMs are formed from the dissolved and unreacted components (e.g. citric acid) in water.[11] As for bubble-like spheres, the possible reason maybe lies in the generation of a gaseous product (e.g. CO_2 or H_2O, etc.) during the decomposition of iron citric as indicated in Figure 1 (E). Since both carbon and Fe_3O_4 are formed in situ, Fe_3O_4 nanoparticles are uniformly dispersed in the walls of MCHMs (Figure 1).

The magnetic properties of the MCHMs were characterised using VSM. As shown in part A of Figure 6, MCHMs (sample HC 2) exhibit ferromagnetism with M_s = 48.2 emu g^{-1}, remnant magnetisation M_r = 9.2 emu g^{-1} and a coercive field H_c = 173 Oe. The reason that M_s is lower

than that of bulk Fe_3O_4 (92 emu g^{-1})[31] can be attributed to the small size of Fe_3O_4 nanoparticles[15,22] and the presence of a nonmagnetic component.

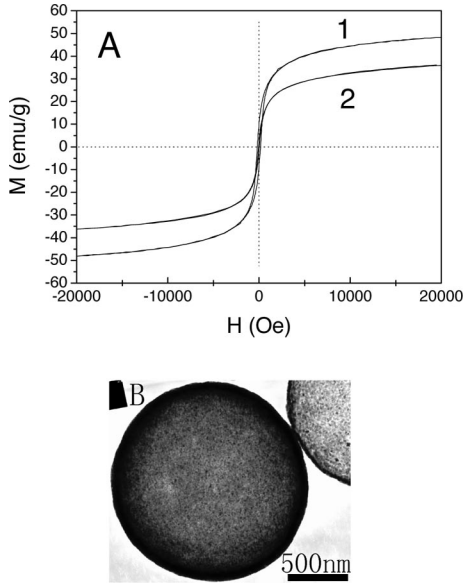

Figure 6. (A) The M–H hysteresis loop for MCHMs (sample HC 2): before (line 1) and after (line 2) acid treatment (pH = 1) at room temperature for 10 d. (B) The TEM image of sample in line 2.

To test the durability of prepared MCHMs under acidic conditions, they were immersed in an excess of aqueous HCl at room temperature. After such treatment (pH = 1) for 10 d, M_s, M_r and H_c of sample HC 2 were 35.9 emu g^{-1}, 2.1 emu g^{-1} and 34 Oe, respectively (Line 2 of Figure 6, A). The TEM images (Figure 6, B) further demonstrate that Fe_3O_4 nanoparticles still exist after acid treatment. On the contrary, HC 0 (i.e. pure iron oxide without carbon protection) gradually dissolved in aqueous HCl (pH = 1). The reason may be that Fe_3O_4 nanoparticles are dispersed in the carbon shell to form MCHMs. Our MCHMs should, therefore, have potential applications in acidic conditions (pH $\geq$ 1) due to their high durability.

The FTIR spectrum was used to identify the functional groups present on the MCHMs' surface and this directly determines their dispersibility in various solvents. Overall, in the range of 1000–3500 cm^{-1}, the spectrum is similar to that of the carbon spheres obtained by the hydrothermal treatment of aqueous glucose.[32] As shown in part A of Figure 7, the bands at 3400 and 1625 cm^{-1} can be assigned to the O–H and C=C functions, respectively. The bands in the 1000–1400 cm^{-1} range can attributed to C–OH stretching and O−H bending vibrations. It should be noted that the bands at 2925 and 2855 cm^{-1}, which can be assigned to hydrogen bonded sp^3 carbon,[18] are stronger than those of the pure carbon sphere[30] while the band at 1710 cm^{-1} (C=O) has almost disappeared. The reason maybe lies in the relatively higher reaction temperature (700 vs. 180 °C) which leads to more complete carbonisation.[18] The band at 570 cm^{-1} can be assigned to Fe_3O_4[18] which is consistent with the results of XRD (Figure 3, A). The dispersibility of MCHMs was investigated by dispersing sample HC 2 in various solvents. Thanks to the presence of OH, C=C and CH groups in MCHMs, they exhibit good dispersibility in both polar and nonpolar solvents, widening their use to a considerable extent. As shown in Figure 7 (B), sample HC 2 can be well dispersed in polar solvents (such as methanol and ethanol) or nonpolar solvents (e.g. tetrachloroethylene) since Fe_3O_4 nanoparticles are uniformly dispersed in a carbon shell to form MCHMs.

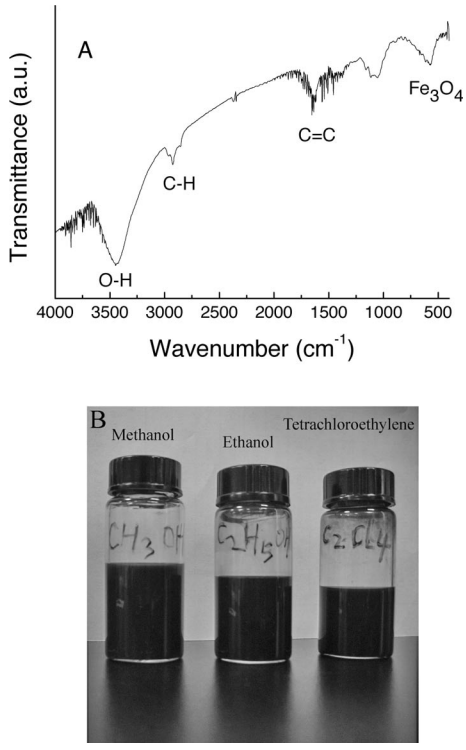

Figure 7. FTIR spectrum of sample HC 2; (B): photographs of sample HC 2 suspensions in methanol, ethanol and tetrachloroethylene (from left to right).

Conclusions

This is the first report of a rapid one-step, template-free, and continuous route leading to MCHMs. Based on the phenomenon that surface enrichment of some components (i.e. formation of hollow spheres) could take place when aerosol pyrolysis of multicomponent systems occurs, MCHMs are produced by USP of aqueous solutions containing ferrous chloride and citric acid. Different from other carbon-magnetite composites, Fe_3O_4 nanoparticles (the size is in the range of 8–20 nm) are dispersed in the shells of MCHMs. Compared with solid carbon-magnetite composites, the lower density, larger surface areas and unique structures with hollow interiors, combined with the good durability and dispersibility of our MCHMs should lead to wide applications in waste removal, immobilisation of biomolecules and catalyst supports etc. This route can probably be extended to prepare other carbon-protected functional composites.

Experimental Section

Preparation of MCHMs by USP: The USP experimental setup was similar to that used by Suslick's group.[24–28] In a typical experiment, citric acid and ferrous chloride were added to deionised water, with magnetic stirring, to form a precursor solution (Table 1). A Yuyue ultrasonic nebuliser was used to nebulise the precursor solution into a fine mist. The furnace temperature was set at 700 °C with a nitrogen flow rate of 2 SLPM (standard litres per minute). After collection in a water-filled beaker, the black product was separated by using a magnet. Finally, a black sample was prepared for further analysis by washing with deionised water and then ethanol three more times.

Acid-Resistance of MCHMs: In order to test their acid-resistance, samples (HC 0 and HC 2) were immersed in an excess of aqueous HCl (pH = 1) at room temperature for 10 d. Different from HC 2, HC 0 gradually dissolved accompanied by formation of a light yellow solution. After washing with deionised water and then ethanol three more times, the black sample was collected for further analysis.

Dispersibility of MCHMs: The dispersibility of carbon-magnetite hollow microspheres in various solvents was investigated as follows: briefly, sample HC 2 (0.05 g) was dissolved in methanol, ethanol and tetrachloroethylene.

Characterisation: X-ray diffraction (XRD) patterns were obtained by using a Rigaku Dmax2000 instrument with Cu-K_α radiation. The morphology of the samples was examined by scanning (SEM, XL30ESEM FEG) and transmission (TEM, JEOL 2010) electron microscopy. The magnetic hysteresis loops of the samples were recorded on a vibrating sample magnetometer (VSM LDJ-9600). Fourier transform infrared spectra (FTIR) of the samples were recorded at ambient temperature on a Nicolet 560 Fourier transform infrared spectrometer with a resolution factor of ± 0.1 cm^{-1} Thermogravimetric analyses (TGA) were carried out using Perkin–Elmer thermal analysis equipment.

Acknowledgments

The current investigations were financially supported by the Hi-Tech Research and Development Program of China (863) (2006AA03Z322, 2007AA021803), the National Natural Science Foundation of China (60572031, 60736001), and the Innovation Foundation of the Chinese Academy of Sciences (CXJJ-178).

[1] F. Caruso, M. Spasova, A. Susha, M. Giersig, R. A. Caruso, *Chem. Mater.* **2001**, *13*, 109–116.
[2] Y. Ding, Y. Hu, L. Y. Zhang, Y. Chen, X. Q. Jiang, *Biomacromolecules* **2006**, *7*, 1766–1772.
[3] F. Teng, T. G. Xu, S. H. Liang, G. L. Buergen, W. Q. Yao, Y. F. Zhu, *Catal. Commun.* **2008**, *9*, 1119–1124.
[4] Y. Q. Zhang, L. L. Li, F. Q. Tang, J. Ren, *J. Nanosci. Nanotechnol.* **2006**, *6*, 3210–3214.
[5] X. Y. Chen, Z. J. Zhang, X. X. Li, C. W. Shi, *Chem. Phys. Lett.* **2006**, *422*, 294–298.
[6] S. Peng, S. H. Sun, *Angew. Chem. Int. Ed.* **2007**, *46*, 4155–4158.
[7] Y. Ding, Y. Hu, X. Q. Jiang, L. Y. Zhang, C. Z. Yang, *Angew. Chem. Int. Ed.* **2004**, *43*, 6369–6372.
[8] Z. B. Huang, F. Q. Tang, *J. Colloid Interface Sci.* **2004**, *275*, 142–147.
[9] Z. B. Huang, F. Q. Tang, *J. Colloid Interface Sci.* **2005**, *281*, 432–436.
[10] X. H. Li, D. H. Zhang, J. S. Chen, *J. Am. Chem. Soc.* **2006**, *128*, 8382–8383.
[11] P. Tartaj, T. González-Carreño, C. J. Serna, *Adv. Mater.* **2001**, *13*, 1620–1624.
[12] V. Salgueiriño-Maceira, M. A. Correa-Duarte, M. Spasova, L. M. Liz-Marzán, M. Farle, *Adv. Funct. Mater.* **2006**, *16*, 509–514.
[13] T. H. Zheng, J. B. Pang, G. Tan, J. B. He, G. L. McPherson, Y. F. Lu, V. T. John, J. J. Zahn, *Langmuir* **2007**, *23*, 5143–5147.
[14] A. Bourlinos, N. Boukos, D. Petridis, *Adv. Mater.* **2002**, *14*, 21–24.
[15] Z. F. Wang, H. S. Guo, Y. L. Yu, N. Y. He, *J. Magn. Magn. Mater.* **2006**, *302*, 397–404.
[16] A. B. Fuertes, M. Serilla, T. Valdés-Solís, P. Tartaj, *Chem. Mater.* **2007**, *19*, 5418–5423.
[17] L. Q. Xu, W. Q. Zhang, Y. W. Ding, Y. Y. Peng, S. Y. Zhang, W. C. Yu, Y. Qian, *J. Phys. Chem. B* **2004**, *108*, 10859–10862.
[18] F. Y. Cao, C. L. Chen, Q. Wang, Q. W. Chen, *Carbon* **2007**, *45*, 727–731.
[19] A. H. Lu, E. L. Salabas, F. Schüth, *Angew. Chem. Int. Ed.* **2007**, *46*, 1222–1244.
[20] J. H. Zhang, J. Du, D. K. Ma, G. C. Xi, X. B. Hu, Y. T. Qian, *Solid State Commun.* **2007**, *144*, 168–173.
[21] A. H. Lu, W. H. Li, N. Matoussevitch, B. Spliethoff, H. Bönnemann, F. Schüth, *Chem. Commun.* **2005**, 98–100.
[22] A. B. Fuertes, T. Valdés-Solís, M. Sevilla, P. Tartaj, *J. Phys. Chem. C* **2008**; *112*, 3648–3654.
[23] T. T. Kodas, M. Hampden-Smith, *Aerosol Processing of Materials*, Wiley-VCH: New York, **1999**, P. 680–685.
[24] N. A. Dhas, K. S. Suslick, *J. Am. Chem. Soc.* **2005**, *127*, 2368–2369.
[25] W. H. Suh, K. S. Suslick, *J. Am. Chem. Soc.* **2005**, *127*, 12007–12010.
[26] S. E. Skrabalak, K. S. Suslick, *J. Am. Chem. Soc.* **2006**, *128*, 12642–12643.
[27] S. E. Skrabalak, K. S. Suslick, *J. Phys. Chem. C* **2007**, *111*, 17807–17811.
[28] J. H. Bang, K. Han, S. E. Skrabalak, H. Kim, K. S. Suslick, *J. Phys. Chem. C* **2007**, *111*, 10959–10964.
[29] Y. F. Zhu, L. X. Zhang, F. M. Schappacher, R. Pöttgen, J. L. Shi, S. Kaskel, *J. Phys. Chem. C* **2008**; *112*, 8623–8628.
[30] J. Kahánková, A. Španová, R. Pantůček, D. Horák, J. Doškař, B. Rittich, *J. Chromatogr. B* **2009**, *877*, 599–602.
[31] K. A. Easom, K. J. Klabunde, C. M. Sorenson, G. C. Hadjipanayis, *Polyhedtron* **1994**, *13*, 1197–1223.
[32] X. M. Sun, Y. D. Li, *Angew. Chem. Int. Ed.* **2004**, *43*, 597–601.

Received: January 21, 2009
Published Online: June 3, 2009

